How does bending the uranyl unit influence its spectroscopy and luminescence

Hanna Oher,[†] André Severo Pereira Gomes,[‡] Richard E. Wilson,[*,¶] David D. Schnaars,[¶] and Valérie Vallet[*,‡]

[†]*Univ. Rennes, CNRS, ISCR (Institut des Sciences Chimiques de Rennes) – UMR 6226, F-35000 Rennes, France*

[‡]*Univ. Lille, CNRS, UMR 8523 - PhLAM - Physique des Lasers Atomes et Molécules, F-59000 Lille, France*

[¶]*Chemical Sciences and Engineering Division, Argonne National Laboratory, Lemont, Illinois 60439, United States*

E-mail: rewilson@anl.gov; valerie.vallet@univ-lille.fr

Abstract

Bent uranyl complexes can be formed with chloride ligands and 1,10-phenanthroline (phen) ligands bound to the equatorial and axial planes of the uranyl(VI) moiety, as revealed by the crystal structures, IR and Raman spectroscopy and quantum chemical calculations. With the goal of probing the influence of chloride and phenanthroline coordination enforcing the bending on the absorption and emission spectra of this complex, spin-orbit time-dependent density functional theory calculations for the bare uranyl complexes as well as for the free UO_2Cl_2 subunit and the $UO_2Cl_2(phen)_2$ ligand were performed. The emission spectra has been fully simulated by ab initio methods and compared to experimental photoluminescence spectra, recorded for the first time for $UO_2Cl_2(phen)_2$. Notably, the bending of uranyl in UO_2Cl_2 and $UO_2Cl_2(phen)_2$

triggers excitations of the uranyl bending mode, yielding a denser luminescence spectrum.

Introduction

The uranyl ion, UO_2^{2+}, on account of its high chemical stability, is ubiquitous in uranium chemistry. Up to a few years ago, the uranyl subunit had been characterized essentially as a linear trans-oxo unit, with very few structures exhibiting $O_{yl}-U-O_{yl}$ bond angles deviating (by few degrees) from linearity.[1,2] The underlying cause for the predominance of linear $O_{yl}-U-O_{yl}$ bonds in UO_2^{2+} is the notable participation of the U 5f and 6p orbitals to the $U-O_{yl}$ bond, while in the iso-electronic ThO_2 molecule 6d and 5f orbitals hybridize and favor a bent geometry.[3,4] Hratchian *et al.*[5] and Schreckenbach *et al.*[6],[7] however proposed the existence of stable 'cis-uranyl' structures in uranyl dihydroxides and tetra-coordinated $[UO_2X_4]^{2-}$ (X = F, Cl, and OH) complexes, with $O_{yl}-U-O_{yl}$ bond angles as acute as 100°. In both linear and bent structures, the 'yl' oxygen atoms carry negative charges making them Lewis bases, with a basicity that increases pairwise with yl-bond weakening as stronger Lewis basis are coordinated in the uranyl equatorial plane.[8,9]

There have been several attempts to synthesize bent actinyl complexes. A simple synthetic route was proposed by Schöne *et al.*[10], in which simply dropping 1,10- phenanthroline (phen) into a uranyl chloride solution in acetone forms the $UO_2Cl_2(phen)_2$ complex, in which the uranyl group is strongly bent (161.8(1)°), and consequently the equatorial plane is broken up. Langer *et al.*[11] have also shown that applying physical pressure on the uranyl-sulfate system can result in a uranyl oxo-salt phase holding a considerably bent uranyl. In 2018, Hayton has catalogued the uranyl complexes that feature a $O_{yl}-U-O_{yl}$ angle smaller than 172°,[2] to which we must add the works by Car[12] and Carter *et al.*[13].

In this work, the focus is on the impact of bending on the uranyl electronic structure. Indeed the ligand induced weakening of uranyl internal bond is expected to impact in the

electronic structures and optical properties of uranyl(VI) complexes. From the detailed work of Zhang and Pitzer[14] on the theoretical side and Denning on the experimental side,[15,16] the spectra of linear uranyl can be explained in terms of excitations from the 'yl-bonding' orbitals (σ_u, σ_g, π_u, σ_g), to the uranium centered non-bonding $5f_\delta$, and $5f_\phi$ orbitals. Typically the spectrum between $20\,000\,cm^{-1}$ and $32\,500\,cm^{-1}$ arises from two, parity conserving orbital excitations, $\sigma_u \rightarrow 5f_\delta$ and $\sigma_u \rightarrow 5f_\phi$, superimposed with vibrational fine structures. While these excited configurations (abbreviated as $\sigma_u\delta_u$ and $\sigma_u\phi_u$) only weakly depend on the nature of the equatorial ligands, they do give rise to numerous excited states due to three perturbations of similar magnitudes : the equatorial ligand field, spin-orbit coupling (SOC) and electron correlation. The various relativistic correlated calculations on the bare uranyl ion reported so far reveal the interplay between SOC and electron correlation, as both the choice of the relativistic framework (4-component, 2-component with SOC treated, or two-step relativistic methods), and the treatment of electron correlation via wave-function theory (WFT) or density functional theory (DFT), may change the relative ordering of the low-lying excited states. These parameters in the calculations also affect the spectroscopic character the lowest state, responsible for the observed luminescence with a long lifetime; it is found to be either a 1_g state (arising from the $^3\Delta_g$ spin-free (SF) triplet state)[14,17,18] or a 2_g state (with a dominant $^3\Phi_g$ character),[18–23] the difference between the various SOC states being small of few hundred wavenumbers if not less, highlighting how challenging the electronic structure of actinide complexes is.[24–26]

Several theoretical studies investigated the characters of the low-lying excited states of uranyl complexed with water,[27,28] halides[19,23,29–31] or acetone ligands,[29] revealing that ligand-field splitting induced by the equatorially bound ligands competes with SOC and electron correlation. This work aims at pushing further the discussion of the impact of structural changes on uranyl spectroscopic properties, by considering the effect of bending the $O_{yl}-U-O_{yl}$ unit, taking the structure of a uranyl bis(1,10-phenanthroline) complex show in Figure 1, $UO_2Cl_2(phen)_2$ originally synthesized by Schöne *et al.*[10], which features a

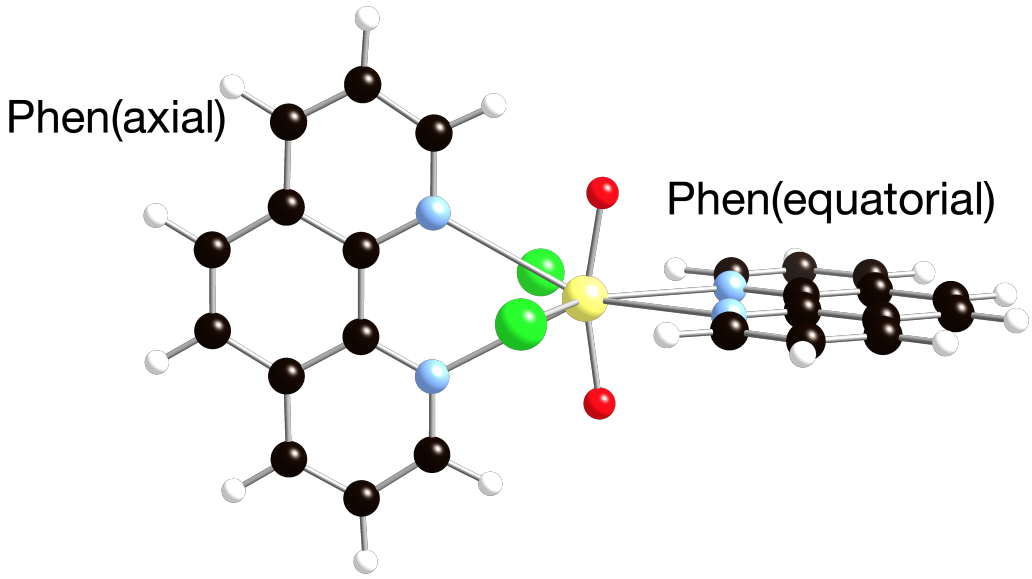

Figure 1: Perspective view of the $UO_2Cl_2(phen)_2$ bent uranyl complex. Color code: yellow (U), red (O), light blue (N), black (C) and white (H).

significantly distorted $O_{yl}-U-O_{yl}$ angle (161.8(1)°).

In this study, we use quantum chemical (QC) methods to easily explore different structural models for the system - bent$-UO_2^{2+}$, UO_2Cl_2, UO_2Cl_2(phen) and $UO_2Cl_2(phen)_2$ – corresponding to a decomposition of the $UO_2Cl_2(phen)_2$ complexes into subunits, and from that assess the relative influence of individual ligand groups (chlorine and phenanthroline groups) on the degree of bending and in the electronic spectrum, as well as to quantify the ligand-field effects of the chlorines the axially and equatorially bound phenanthroline groups, and their importance to the nature of the low-lying excited states. The computational data are compared to experimental luminescence and vibrational spectroscopic data collected on $UO_2Cl_2(phen)_2$ that is synthesized by an alternative method to that previously reported by Schöne *et al.*[10].

Computational Details

The geometry optimizations of the $UO_2Cl_2(phen)_2$ complex in its ground state (singlet state) and its lowest excited triplet state were carried out with the Gaussian 16 software,[32] in the gas phase with density functional theory (DFT) and the PBE0 functional[33,34] with D3 dispersion correction with Becke damping to account for non-covalent interactions,[35,36] which turned out to be important to obtain interatomic uranyl-ligand bond distances matching the experimental data within about 0.03 Å (See also Table S1 in the SI). Note that all calculations (geometry optimizations and calculations of absorption and emission energies) have been performed in the gas-phase, with arguments detailed in the Section 1. In addition to that, we have performed optimizations on its subunits UO_2Cl_2, $UO_2Cl_2(phen)_{ax}$, $UO_2Cl_2(phen)_{eq}$. For all complexes, two configurations for the O-U-O bond angle were investigated: one in which it was allowed to relax and another where it was constrained to be equal to 180 degrees. In the later cases, one imaginary vibrational mode corresponding to the bending of the uranyl moiety always appear confirming that the linear geometries are transition-state structures

that relax to bent structures when the linearity constraint is lifted. The U atom is described using a small core relativistic pseudopotential (60 core electrons)[37] with the corresponding segmented basis set including a 3g polarization functions;[38,39] all other atoms were described with def2-TZVP basis sets.[40] To determine the energy cost of bending we have also used the single-reference MP2 post-Hartree-Fock method to perform single-point calculations at the PBE0-D3 optimized geometries. Note that uranyl complexes are expected to have marginal multireference character,[21] and that MP2 is expected to yield more accurate relative energies than any functional of the density (See Table S2 and discussions in Refs. 41–43). In these MP2 calculations the core orbitals were frozen, namely the 1s of first row elements, the 1s, 2s, 2p of chlorine atoms, and the 5s, 5p, 5d pseudovalence orbitals of uranium.

Uranium–ligand chemical bonds were analyzed through the topology of the electronic density with the QTAIM theory[44,45] implemented in the AIMall package.[46] Natural population analysis and Wiberg bond order have been computed with the NBO7 program.[47]

To investigate how the bending of the uranyl moiety influences the energy position and nature of low-lying excited states of $UO_2Cl_2(phen)_2$, we have chosen a computationally affordable yet reliable approach, that is using time-dependent DFT (TDDFT) combined with the range-separated hybrid CAM-B3LYP functional[48] as it has proven to be more reliable than other hybrid functionals for the absorption and emission energies of small to large uranyl(VI) complexes,[20,21,49–54] including simulations of core-energy levels.[55] The ADF program[56–58] was used for all TDDFT calculations with the full (non-ALDA) kernel, and the lowest 16 electronic states were computed. Calculations are performed in the gas phase for the linear and bent uranyl complexes. Relativistic effects were included via either the Scalar relativistic (SR) or spin-orbit (SO) ZORA Hamiltonians.[59–61] We have employed basis sets of triple-zeta plus polarization (TZ2P) quality for all atoms without freezing core orbitals.[62]

The theoretical vibronic progressions of the UO_2Cl_2, $UO_2Cl_4{}^{2-}$ and $UO_2Cl_2(phen)_2$ luminescence have been computed with the `ezSpectrum 3.0`[63] software. The Franck-Condon factors (FCFs) were obtained based on the structures and the full set of vibrational modes

of the ground and first low-lying excited state structures of complexes of interest following the methodology deduced previously and reported elsewhere.[51–53] The first low-lying excited state structures were obtained using the TDDFT method as implemented in G16[32] using the same PBE0-D3 functional as for the ground-state description. The temperature for the FCFs calculations was set to repeat the experimental conditions, thus 4 K for UO_2Cl_2[64] and 80 K for $UO_2Cl_4^{2-}$ and $UO_2Cl_2(phen)_2$ complexes. For the simplicity of the experimental luminescence spectra assignments, the second set of calculations was performed at 4 K to minimize the contributions from the thermally active vibrational modes.

Experimental Details

CAUTION! ^{238}U*, is an* α*-emitting radionuclide. This material was handled in a radiological facility under radiological controls* All reactions were conducted under ambient atmospheric conditions except where noted. All materials were used as received from commercial sources. KBr was ground and dried for a minimum of 48 hours at 120 °C. $(Ph_4P)_2UO_2Cl_4 \cdot 2\,MeCN$, was synthesized as described previously,[65] and washed three times with 200 µL of H_2O to remove residual HCl.

Synthesis

In a 2 mL shell vial, 30.6 mg mg (0.026 mmol) of $(Ph_4P)_2UO_2Cl_4 \cdot 2\,MeCN$ was dissolved in 750 µL of MeCN forming a yellow-green solution To this solution was added 500 µL of MeCN containing 31.0 mg (0.156, 6 equiv.) of 1,10-phenanthroline·H_2O without color change. This solution was warmed in a water bath at 50 °C and allowed to cool slowly to room temperature resulting in the deposition of yellow-green single crystals (9.8 mg, 54 % yield). For isotopic exchange of the -yl oxygen atoms to aid in spectral assignment of the vibrational structure, ^{18}O labeled water was used in the preparation of the $(Ph_4P)_2UO_2Cl_4 \cdot {}_2CH_3CN$ starting material. Prior to crystallization, the capped sample was irradiated under UV light

to facilitate uranyl-oxo ligand exchange with the ^{18}O water. This salt was used in subsequent synthesis of the labeled $UO_2Cl_2(phen)_2$ complex. $Cs_2UO_2Cl_4$ was prepared according to literature methods.[66]

X-ray Crystallography

Single crystal X-ray diffraction data were collected using a Bruker APEX II diffractometer and detector with a Quazar Microfocus source, $Mo_{K\alpha}$ radiation. Single crystals were affixed to a fine glass capillary using a quick drying epoxy. Data were collected at 100 K using an oxford Cryosystems Cryostream 700 device. Data were corrected for absorption using SADABS,[67] structures were solved using SHELXS and refined with SHELXL.[68] The crystallographic data including the structure factors have been deposited with the Cambridge Crystallographic Data Centre under accession code 2245382.

Spectroscopy

FT-IR spectra were collected on pressed pellets containing 1-5 wt% of the sample diluted into dry KBr powder using a Nicolet 870 FT-IR spectrometer. Data were collected as an average of 16 scans over 4000 - 400 cm^{-1} and a resolution of 2 cm^{-1}. Raman data were collected from randomly oriented single crystals using circularly polarized 785 nm laser light on a Renishaw inVia Raman microscope system. The FT-IR and Raman spectra of the complexes are presented in the SI (Figure S1, Figure S2).

Photoluminescence of the uranyl salts $Cs_2UO_2Cl_4$ and $UO_2Cl_2(phen)_2$ was collected using the 442 nm (22 624 cm^{-1}) excitation line of a He-Cd laser on the Renishaw inVia Raman microscope. Emission was collected on randomly oriented single crystals using circularly polarized radiation with a defocused and attenuated laser beam to prevent sample burning and detector saturation. The emission wavelengths were recorded from 100 to 8000 cm^{-1} lower in frequency relative the excitation wavelength at 293 K and 80 K. Samples were mounted on custom tantalum crucibles to which a glass cover slip had been epoxided. The

temperature was thermostated using a Linkham 600 series sample stage with flowing liquid nitrogen.

Results and Discussion

Synthesis and crystallographic structure

Prior reports of uranyl molecules whose O≡U≡O bond angle deviates significantly from linearity are known in the literature.[2,10,12,13] The synthesis reported here was conducted independently exploiting the salts $(Ph_4P)_2UO_2Cl_4{\cdot}_2CH_3CN$ salts and their solvates, reported previously,[65] as starting materials in warm MeCN solutions under ambient conditions with an excess of 1,10-phenanthroline. Prior synthetic reports have employed alternate solvents, e.g. acetone, hydrothermal aqueous methods and carboxylic acids in the presence of 1,10-phenanthroline to arrive at bent actinyl geometries, thus highlighting the potential richness of the synthetic phase space of these disorted -yl units.

Results of the X-ray crystallographic refinements shown in Table 1 demonstrate that the $UO_2Cl_2(phen)_2$ complex reported here is isostructural with that previously reported. Table 1 also presents the experimentally measured bond distances and angles for the reported complex.

Structure and bonding in $UO_2Cl_2(phen)_2$

The geometry optimization of the $UO_2Cl_2(phen)_2$ molecule in the gas phase (DFT-PBE0-D3) converges to a bent molecule (See Table 2), with U-Cl bond distances perfectly matching the experimental values; the U-N bonds are slightly longer by 0.03 Å than in the crystal structure. The O≡U≡O angle is computed to be as bent (162.7°) as in the crystal (161.7°). This indicates that the significant bending of the O≡U≡O unit is not induced by the crystal packing but rather by the first coordination sphere. Phenanthroline preferably binds UO_2Cl_2 in the equatorial position (See binding energies in Table S3 of the SI). However the axial

Table 1: Crystallographic parameters and experimentally measured bond lengths (Å) and angles (°) for $UO_2Cl_2(phen)_2$ from the single crystal X-ray diffraction refinements.

Crystallographic param.		Bond lengths (Å) and angles (°)			
		U≡O	O≡U≡O	U-Cl	U-N
empirical formula	$C_{24}H_{16}Cl_2N_4O_2U$	1.773(3)	161.71(11)	2.6634(9)	2.647(3)
formula weight ($g\,mol^{-1}$)	701.34	1.780(3)		2.6846(9)	2.668(3)
crystal habit	prismatic				2.755(3)
color	yellow				2.767(3)
size (mm)	0.12 x 0.07 x 0.06				
crystal system	triclinic				
space group	$P\bar{1}$				
V ($Å^3$)	1095.85(14)				
a (Å)	8.5359(6)				
b (Å)	9.4193(7)				
c (Å)	14.5821(11)				
α (°)	79.9640(10)				
β (°)	89.7740(10)				
γ (°)	71.9100(10)				
Z	2				
T (K)	100				
ρ ($g\,cm^{-3}$)	2.125				
μ (mm^{-1})	7.681				
GoF	1.017				
R_1	0.0369				
wR^2	0.0583				

Table 2: Symmetric (ν_s) and asymmetric (ν_{as}) vibrational modes of the uranyl ions (cm^{-1}), bond length (Å) and angles (°) for $UO_2Cl_2(phen)_2$ and the subunits UO_2Cl_2, $UO_2Cl_2(phen)_{ax}$, $UO_2Cl_2(phen)_{eq}$ optimized at the DFT-PBE0-D3 level of theory. ΔE (in $kJ\,mol^{-1}$) stands for the MP2 electronic energy difference between the linear and bent structures, the most stable structures being bent.

Complex	Geom.	ν_s	ν_{as}	U≡O	O≡U≡O	U−Cl	U−N_{ax}	U−N_{eq}	ΔE
UO_2Cl_2	Bent	949	1021	1.733	169.2	2.510(3)	-	-	0.0
	Linear[a]	959	1032	1.729	180.0	2.514	-	-	8.7
$UO_2Cl_2(phen)_{ax}$	Bent	898	966	1.751	153.1	2.649	2.718	-	0.0
	Linear[a]	936	1006	1.735	180.0	2.553	2.975	-	24.0
$UO_2Cl_2(phen)_{eq}$	Bent	933	1003	1.741	173.5	2.602	-	2.584	0.0
	Linear[a]	936	1007	1.740	180.0	2.606	-	2.588	1.1
$UO_2Cl_2(phen)_2$	Crystal.	820	890	1.778(3)	161.7	2.67(1)	2.759(5)	2.65(1)	
	Bent	896	957	1.754	162.7	2.660	2.789	2.680	0.0
	Linear[a]	918	988	1.743	180.0	2.651	3.004	2.669	33.5

[a] O≡U≡O angle constrained to 180°; one imaginary mode corresponding to the bending of the uranyl moiety.

phenanthroline group is the one that induces a significant bending. If the uranyl unit is forced to be linear, the bond distances to the chlorides and the "equatorial" phenanthroline group are unchanged, while the "axial" phenanthroline group that lie in the same plane as the yl-oxygen is pushed away at distances of 3.02 Å. From Table S3 this severe geometrical change corresponds to an energy gain of $33.5\,kJ\,mol^{-1}$ in agreement with the value $29.8\,kJ\,mol^{-1}$ reported by Schöne *et al.*[10]

Interestingly the optimal geometries of all subunits UO_2Cl_2, $UO_2Cl_2(phen)_{ax}$, $UO_2Cl_2(phen)_{eq}$ also lead to a bent uranyl. The largest distortion from linearity being found for the $UO_2Cl_2(phen)_{ax}$, with an angle of 153.1°, paired with a significant energy stabilization upon bending, $24.0\,kJ\,mol^{-1}$, almost as large as in the bi-phen complex. The computed symmetric and asymmetric vibrational frequencies of $UO_2Cl_2(phen)_2$ are larger than the experimental values, but the split between the two $62\,cm^{-1}$ agrees with the value $70\,cm^{-1}$ reported experimentally.

To investigate further the $U{\equiv}O_{yl}$ chemical bond and its changes as it bends, we have applied the quantum theory of atoms-in-molecules (QTAIM), which probes the density at

the bond critical point between pairs of atoms that are bonded to one another. One can classify the type of chemical bonding by the density properties at the bond critical point (BCP), namely the value of the density ρ, the sign of the Laplacian $\nabla^2\rho$ and the energy density H, and the comparison of the ratio between the potential energy density and the kinetic energy density at the BCP ($|V|/G$) to 1, all of which are listed in Table S4, together with the delocalization index $\delta(\mathrm{U,L})$ and the Wiberg Bond order that both measure the U−L bond order. In the stable $UO_2Cl_2(phen)_2$ bent geometry, the BCP parameters of the interactions between uranium and both the chlorides and the phenanthroline groups are very close to those reported by Vallet *et al.*[8] for $[UO_2F_4]^{2-}$ or $UO_2Cl_4{}^{2-}$ complexes, thus corresponding to ionic interactions. However for both equatorial bonds, the ratio ($|V|/G$) is larger than 1. With this we can qualify both U−N and U−Cl bonds as mostly ionic with some covalency, the latter being somewhat more covalent than the former both from the ($|V|/G$) ratio values and the bond-order values.

The U≡O_{yl} BCP characteristics ρ, $\nabla^2\rho$, H, and the bond orders are slightly smaller in the bent structures than in the linear ones, indicating a corresponding reduction of the strength of the U≡O_{yl} upon bending in line with a bond lengthening of 0.01 Å. The Natural Population Analysis also points out that the population of the uranium 6d orbitals increases while that of the 5f orbitals decreases in the bent structure as compared to the linear molecule. This is expected as 6d orbitals take a more prominent role in bonding for bent molecules such as ThO_2,[3,69] or transition metals Mo(VI) and W(VI) oxides.[70] We stress though that the changes in the U≡O_{yl} bond upon bending are marginal, thus suggesting that the bending is mostly induced by the electrostatic repulsion of both the chloride and phenanthroline ligands.

The nature of the low-lying electronic states of $UO_2Cl_2(phen)_2$

The low-lying excited states of uranyl complexes are dominated by excitations out of the σ_u U≡O bonding orbital (label referring to the linear $UO_2{}^{2+}$ unit in the scalar relativistic

Table 3: SO-TDDFT/CAM-B3LYP vertical transition energies (in cm^{-1}) in linear UO_2^{2+} and bent UO_2^{2+} (computed at the $UO_2Cl_2(phen)_2$ PBE0-D3 geometries) and $UO_2Cl_4^{2-}$ computed at the crystal geometry. Experimental data for $Cs_2UO_2Cl_4$ from Ref. 15,16.

linear UO_2^{2+} (r(U$-$O$_{yl}$)=1.754 Å)		bent UO_2^{2+} (r(U$-$O$_{yl}$)=1.743 Å)	
Trans.	ΔE	Trans.	ΔE
$\sigma_u \rightarrow \phi$	14 097	$\sigma_u \rightarrow \phi$	13 500
$\sigma_u \rightarrow \phi$	15 447	$\sigma_u \rightarrow \phi$	14 801
$\sigma_u \rightarrow \delta$	17 007	$\sigma_u \rightarrow \delta$	16 572
$\sigma_u \rightarrow \delta$	18 892	$\sigma_u \rightarrow \delta$	18 451
$\sigma_u \rightarrow \phi$	20 738	$\sigma_u \rightarrow \phi$	20 117
$\sigma_u \rightarrow \delta(78\%) + \phi(18\%)$	22 007	$\sigma_u \rightarrow \delta(74\%) + \phi(21\%)$	21 541
$\sigma_u \rightarrow \phi(80\%) + \delta(16\%)$	24 002	$\sigma_u \rightarrow \phi(76\%) + \delta(19\%)$	23 212
$\pi_u \rightarrow \phi$	27 645	$\pi_u \rightarrow \phi$	26 480

$UO_2Cl_4^{2-}$

Trans.	ΔE	ΔE^{exp}	$\Delta\Delta E$
$\sigma_u(54\%) + Cl(39\%) \rightarrow \delta(82\%) + \phi(11\%)$	19 553	20 096	-543
$\sigma_u(54\%) + Cl(39\%) \rightarrow \delta(84\%) + \phi(11\%)$	19 553	20 097	-544
$\sigma_u(55\%) + Cl(47\%) \rightarrow \phi(69\%) + \delta(21\%)$	19 880	20 407	-527
$\sigma_u(57\%) + Cl(36\%) \rightarrow \phi(60\%) + \delta(32\%)$	20 578	21 316	-738
$\sigma_u(58\%) + Cl(34\%) \rightarrow \phi(72\%) + \delta(11\%)$	21 528	22 026	-498
$\sigma_u(57\%) + Cl(34\%) \rightarrow \phi(72\%) + \delta(11\%)$	21 596	22 076	-480
$\sigma_u(58\%) + Cl(36\%) \rightarrow \phi(45\%) + \delta(45\%)$	22 149	22 406	-257
$\sigma_u(59\%) + Cl(35\%) \rightarrow \delta(54\%) + \phi(26\%)$	22 334	22 750	-416

framework) into the uranium centered non-bonding orbitals labeled ϕ, and δ. The lowest lying luminescent state can either have a ($\sigma_u\delta$) or ($\sigma_u\phi$) character, depending on how ligand-field affects the orbitals involved in the excitation. In the cases of UO_2F_2,[28] and $[UO_2Cl_3]^-$[71] and the uranyl tetrahalides,[31,72] the luminescent state has a ($\sigma_u\delta$) character. To check whether our choice of basis sets and DFT functional (CAM-B3LYP) reproduces that known observation, we have computed the spectrum of $UO_2Cl_4^{2-}$ using the crystal structure of $[PPh_4]_2UO_2Cl_4 \cdot 2\,MeCN$.[65] The assignment of the computed transition energies (See Table 3) does agree with the fact that the luminescent state corresponds to an excitation to a δ orbital, noting that the excitation involves in almost equal amounts the σ_u uranyl orbital and the chloride 3p orbitals. It is also noteworthy the excellent agreement between the computed transition energies and experimental data for $UO_2Cl_4^{2-}$ as noted previously by Gomes *et al.*[31] for the same system and by Tecmer *et al.*[50] and Oher *et al.*[51–53] for other uranyl complexes. We shall here remark that the onset of valence excitation energies for UO_2^{2+} appears several thousands wavenumbers lower than in $UO_2Cl_4^{2-}$. As noted earlier, for UO_2^{2+}, TDDFT (CAM-B3LYP), in comparison to wavefunction methods, places the first excited states at lower energies than complete active space second-order perturbation theory (CASPT2) and intermediate Hamiltonian Fock-space coupled cluster (IHFSCC) methods.[21] The origin of these differences between the two methods has not been elucidated and calls for further investigations for the bare uranyl itself and for the "small" UO_2Cl_2 molecule, as it may induce a bias in the emission energy of the UO_2Cl_2, as discussed later.

Prior to discussing the nature of the low-lying electronic states in the system of interest, $UO_2Cl_2(phen)_2$, we wish to quantify in a systematic way the relative importance various effects, such as 1) the bending of the uranyl subunit by comparing the spectrum of the bare uranyl in a linear and bent conformations; 2) the ligand-field of the chloride ligands in UO_2Cl_2, and that of the phenanthroline groups; and 3) the strength of spin-orbit coupling by comparing two-component (SO) and scalar relativistic (SR) results. The ten lowest TDDFT SO-excited states and their transitions, are listed in Table 3 and Table 4, while the corre-

Table 4: SO-TDDFT/CAM-B3LYP vertical transition energies (in cm^{-1}) and oscillator strengths in the UO_2Cl_2, and $UO_2Cl_2(phen)_2$ molecules computed at the PBE0-D3 geometries.

UO_2Cl_2		
Trans.	ΔE	f
$\sigma_u(32\%) + \mathrm{Cl}(62\%) \rightarrow \phi(87\%) + \delta(9\%)$	17 303	1.95×10^{-5}
$\sigma_u(31\%) + \mathrm{Cl}(63\%) \rightarrow \phi(93\%) + \delta(3\%)$	17 466	8.70×10^{-5}
$\sigma_u(35\%) + \mathrm{Cl}(59\%) \rightarrow \delta(77\%) + \phi(18\%)$	17 979	7.95×10^{-13}
$\sigma_u(33\%) + \mathrm{Cl}(58\%) \rightarrow \delta(77\%) + \phi(18\%)$	17 990	8.12×10^{-6}
$\sigma_u(28\%) + \mathrm{Cl}(63\%) \rightarrow \phi(62\%) + \delta(29\%)$	18 374	1.40×10^{-12}
$\sigma_u(29\%) + \mathrm{Cl}(64\%) \rightarrow \phi(71\%) + \delta(19\%)$	18 475	8.11×10^{-7}
$\sigma_u(33\%) + \mathrm{Cl}(59\%) \rightarrow \delta(69\%) + \phi(7\%)$	19 814	9.42×10^{-4}
$\sigma_u(30\%) + \mathrm{Cl}(63\%) \rightarrow \delta(77\%) + \delta(2\%)$	20 159	1.26×10^{-6}
$UO_2Cl_2(phen)_2$		
$\sigma_u + \mathrm{Cl} \rightarrow \phi/\pi^*_{(phen)_{ax}}(64\%) + \delta/\pi^*_{(phen)_{ax}}(10\%)$	19 338	1.02×10^{-4}
$\sigma_u + \mathrm{Cl} \rightarrow \phi/\pi^*_{(phen)_{ax}}(81\%) + \delta/\pi^*_{(phen)_{ax}}(2\%)$	19 507	3.49×10^{-5}
$\sigma_u + \mathrm{Cl} \rightarrow \phi/\pi^*_{(phen)_{ax}}(81\%) + \delta/\pi^*_{(phen)_{ax}}(2\%)$	19 601	0.0
$\sigma_u + \mathrm{Cl} \rightarrow \delta/\pi^*_{(phen)_{ax}}$	19 656	1.71×10^{-7}
$\sigma_u + \mathrm{Cl} \rightarrow \phi/\pi^*_{(phen)_{ax}}(75\%) + \delta/\pi^*_{(phen)_{ax}}(5\%)$	20 516	0.0
$\sigma_u + \mathrm{Cl} \rightarrow \phi/\pi^*_{(phen)_{ax}}(75\%)$	20 666	3.73×10^{-5}
$\sigma_u + \mathrm{Cl} \rightarrow \delta/\pi^*_{(phen)_{ax}}(52\%) + \phi/\pi^*_{(phen)_{ax}}(9\%)$	21 515	7.28×10^{-4}
$\sigma_u + \mathrm{Cl} \rightarrow \delta/\pi^*_{(phen)_{ax}}(56\%) + \delta/\pi^*_{(phen)_{eq}}(6\%)$	21 983	1.70×10^{-6}

sponding SR values, as well as the TDDFT results, are reported in Supporting Information (Table S5, Table S6, Table S7). We note that a comparison of TDDFT and TDDFT/TDA (Tamm-Dancoff Approximation) results has been suggested in the literature[73] as a way to differentiate local and charge-transfer excitations – discrepancies between the results of the two calculations being the signature of charge-transfer excitations. We report differences up to 600 cm^{-1} between TDDFT and TDDFT/TDA results for UO_2Cl_2 (See Table S8), thus indicating that although the excited states involve both chloride 3p orbitals and the uranyl σ_u, the charge-transfer per say is not significant, and is well captured by the range-separated CAM-B3LYP functional.

Further evidence that contributions from charge-transfer should not play a significant role for the low-lying spectrum of uranyl-containing complexes with chloride ligands is found in the relatively small differences in excitation energies between calculations for the $UO_2Cl_4^{2-}$ molecule and for the UO_2^{2+} ion embedded into the potential of the four chlorides in the equatorial plane,[31] since in the latter transitions to or from the chloride ligands are absent by construction. This embedding model can be considered as a rather flexible analogue to a ligand field treatment, based entirely on DFT calculations and in which not only electrostatic but electron correlation and orthogonalization effects are taken into account. We observe a fairly systematic redshift, of about 1000 cm^{-1}, for the lowest 12 excited states of the embedded UO_2^{2+} model. The differences in spacing between the different excited states are somewhat larger for the three four lying excited states, reaching about 600 cm^{-1}, but fall down to less than 100 cm^{-1} for higher-lying states.

In $UO_2Cl_2(phen)_2$, the U≡O bond distances are longer by almost 0.1 Å than those optimized for the bare uranyl ion in its electronic ground state,[18] and very close to the optimal geometry of the first-excited (luminescent) state.[22] The transition energies reported in Table 3 are thus closer to emission energies for the bare uranyl species, and they cannot be directly compared to the values reported in the literature.[18,22]

In the bare uranyl unit (Table 3), the first seven excited states arise from excitations

from the σ_u highest occupied molecular orbital (HOMO) into the non-bonding δ, ϕ manifold, followed by transitions out of the π_u orbitals. Bending stabilizes the transitions to the ϕ spinors by $597\,\mathrm{cm}^{-1}$ at most, while the latter are stabilized by about $435\,\mathrm{cm}^{-1}$. However, bending the uranyl unit maintains the $\sigma_u\phi$ character of the lowest luminescent state.

With the two coordinated chlorides, all transitions are shifted up by about $3000\,\mathrm{cm}^{-1}$ as compared to those of the bent $UO_2{}^{2+}$ (See Table 3 and Table 4); still the lowest excited states correspond to excitation to the ϕ non-bonding orbital as in the bare uranyl unit. In UO_2Cl_2, the nature of accepting non-bonding orbitals in the first 8 excited states resembles that of the bare bent uranyl cation, but doubly occupied 3p orbital of the coordinated chlorines, that appear as the LUMO, contribute to the excitations up to about 60 % and mix in with contributions from the doubly occupied σ_u orbital that lie below the chloride 3p manifold. Note that because of limitations in the active space size, the preceding SO-CASPT2 by Su *et al.*[22] calculations did not include the chloride 3p orbitals, thus making it impossible to see any such contributions to the transitions.

The binding of the phenanthroline groups shifts all transition energies further up, so that these now start at $19\,338\,\mathrm{cm}^{-1}$, in line with the experimentally recorded spectrum. It is noteworthy that two lowest states with ϕ character are only separated by about $318\,\mathrm{cm}^{-1}$ from the next two states with δ character. The molecular orbitals participating to the four lowest excited states are shown on Figure 2, revealing that the orbital out of which the electrons are excited from is centered on the UO_2Cl_2 subunit involving a mixture of chloride 3p orbitals and the uranyl σ_u. For the lowest two excited states, the accepting orbital has a uranium $5f_\phi$ character. The third and fourth state, the accepting spinor has a dominant $5f_\delta$ character. Moving up in energy, a spinor with π^* of the axial phenanthroline group mixes in. In that sense, the low-lying excitations remain strongly localized on the UO_2Cl_2 subunit, with a character that resembles the $[\sigma_u + \mathrm{Cl}(3p) \rightarrow \mathrm{U(f)}]$ but there are now non-negligible contributions from spinors/orbitals located over the axial phenanthroline group.

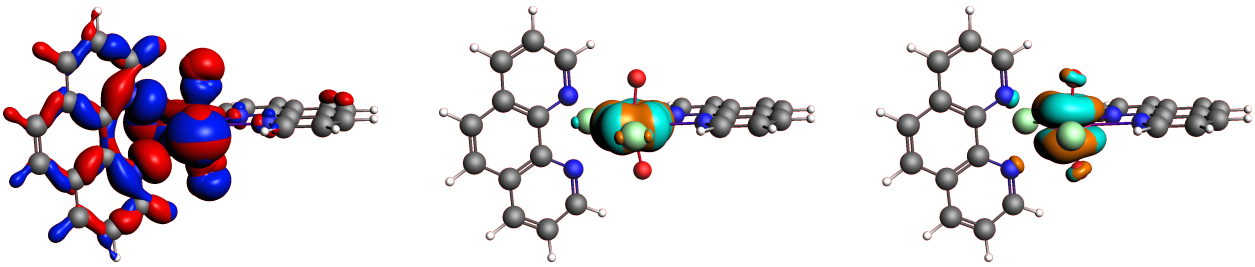

(a) (b) (c)

Figure 2: Molecular spinors: a) occupied orbital which the electron is excited from; b) empty orbital accepting the electron in the first three excited state; c) empty orbital accepting the electron in the fourth excited state. Isosurface values are ±0.03 au.

Ligand-field effects and spin-orbit coupling

As discussed by Su *et al.*[22] the nature of the luminescent state is determined by the competition between SO-coupling that stabilizes more the ϕ orbitals than the δ, and the ligand-field splitting that may destabilize the ϕ and δ orbitals depending on the ligands. It is possible to quantify these two effects: the ligand-field splitting can be measured by the difference of the SR transition energies for states with ϕ/δ characters in a molecular complex with respect to the corresponding ones in the bare uranyl species; the spin-orbit stabilization is simply computed as the difference between the lowest state with a dominant ϕ/δ and its SR triplet counterpart.

Table 5: Energy gap ($E_{SR}(\delta) - E_{SR}(\phi)$) between the triplet SR states dominated by excitations into the δ and ϕ orbitals (positive values mean that the δ are above the ϕ states); $\Delta E_{LF}(\delta, \phi)$ is the ligand field splitting of the SR states dominated by excitations into the δ and ϕ orbitals; $\Delta E_{SO}(\delta, \phi)$ is the spin-orbit stabilisation of the SR states dominated by excitations into the δ and ϕ orbitals. All values are in cm^{-1} and computed in the gas phase.

Compound	$E_{SR}(\delta) - E_{SR}(\phi)$	$\Delta E_{LF}(\phi)$	$\Delta E_{LF}(\delta)$	$\Delta E_{SO}(\phi)$	$\Delta E_{SO}(\delta)$
linear UO_2^{2+}	1433			−3580	−2103
bent UO_2^{2+}	1743			−3483	−2153
$[UO_2Cl_4]^{2-}$	−3095	7403	2875	−5199	−2432
UO_2Cl_2	−1053	3547	1060	−3920	−2190
$UO_2Cl_2(phen)_2$	−1657	5959	2869	−4297	−2377

As revealed by the values of Table 5, in the bare linear and bent uranyl the ϕ SR states

lie about 1433 to 1743 cm^{-1} below the δ states, in the linear and bent moiety, respectively. Its SO stabilization being larger (about -3580 to $-3483\,cm^{-1}$) than that of the δ state (about -2153 to $-2103\,cm^{-1}$), the lowest SO excited state has a ϕ character. In $UO_2Cl_4^{2-}$, the state ordering is different, as the four chlorides destabilize the ϕ SR states far more, $7403\,cm^{-1}$, than the δ states, $2875\,cm^{-1}$. This strong destabilization of the ϕ SR states is not compensated by the larger SO energetic stabilization. As a result, the first excited state has a δ character and involves excitations out of both the σ_u uranyl orbital and the chloride 3p orbitals. In UO_2Cl_2 and $UO_2Cl_2(phen)_2$, the ligand-field effect is not as strong as in the tetra-chloride uranyl complex; the chloride and phenanthroline groups destabilize the ϕ SR states far more than the δ states (3547 versus $1060\,cm^{-1}$ in UO_2Cl_2, and $5959\,cm^{-1}$ versus $2869\,cm^{-1}$ in $UO_2Cl_2(phen)_2$. The SO stabilization effects being almost the same as in the bare unit, that is about $1920\,cm^{-1}$ larger for the ϕ states than the δ states, thus placing the SO states with a δ character few cm^{-1} higher than the ϕ ones.

The excellent agreement between the computed and experimental vertical absorption energies for $UO_2Cl_4^{2-}$ (See Table 3) demonstrates that the energy spacing within the excited state manifold is accurately captured by CAM-B3LYP. Taken together with the results for the embedded model[31] for UO_2^{2+} mentioned above, these results make us confident about the ability of CAM-B3LYP to accurately capture the effects ligand-field and SO splittings onto the low-lying valence states of uranyl complexes.

Emission spectra of UO_2Cl_2 and $UO_2Cl_2(phen)_2$

Luminescence spectroscopy is one of the experimental techniques that can probe a chemical interaction of U(VI) with the equatorial ligands of a complex. Uranium (VI) complexes display specific luminescence features with characteristic band shapes that mostly depend on chemical composition of the closest environment of uranyl unit. The luminescence spectrum of UO_2Cl_2 has been recorded previously at 4 K in Ar matrix conditions and reported by Jin *et al.*[64] (Figure 3(a)). In our study the $UO_2Cl_2(phen)_2$ luminescence spectra are obtained

at 80 K and 293 K as it is shown on Figure 3(b). Both compounds exhibit the same type of progression with the difference in spectral lines resolution that mostly depends on the contributions from the thermally active bands induced by the temperature effects.[74]

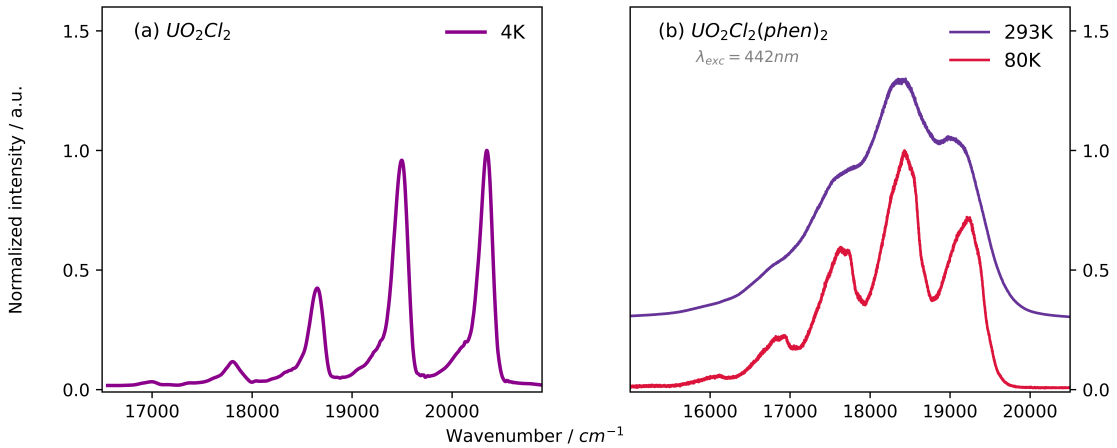

Figure 3: The normalized experimental luminescence spectra of (a) UO_2Cl_2 at 4 K reconstructed with permission from Jin *et al.*[64] – Copyright 2009 American Chemical Society; and (b) $UO_2Cl_2(phen)_2$ spectra recorded at 80 K and 293 K after 442 nm excitation.

Experimentally, the luminescence of uranium(VI) complexes originates at 20 343 cm^{-1} for UO_2Cl_2 and 19 135 cm^{-1} in the case of $UO_2Cl_2(phen)_2$. Such a shift is observed because of the changes in the overall basicity of the complex. At a low-temperature Ar as the Lewis basis can bind to uranium,[22] but the presence of a lone pair of electrons of nitrogen of phenanthroline ligands makes it more basic as compared to Ar that causes a luminescence origin shift to lower wavenumbers. For instance, in $UO_2Cl_4^{2-}$ the nature of equatorial ligands is the same as in UO_2Cl_2 and its experimental luminescence origin corresponds to 20 096 cm^{-1}[75] and matches well with the value obtained for UO_2Cl_2. In general, the luminescence spectrum of uranium(VI) complexes results from the electronic transition from the low-lying excited states to the ground state coupled to vibronic progression. Whereas the overall nature of uranium(VI) luminescence is still a topic for discussion since it might consist of radiative and non-radiative processes, the direct comparison between theoretical and experimental electronic transition energies is misleading. Yet here we could discuss the nature of the radiative

part of UO_2Cl_2 and $UO_2Cl_2(phen)_2$ luminescence deduced from theoretical calculations of emission energies and vibronic progressions.

Theoretical vertical emission energies are obtained from the $(\sigma_u\phi)$ lowest excited state structures of UO_2Cl_2 and $UO_2Cl_2(phen)_2$ complexes and reported in Table 6. While for the large $UO_2Cl_2(phen)_2$ complex, the computed and experimental data, $18\,464\,cm^{-1}$ and $19\,135\,cm^{-1}$, respectively, closely match, for UO_2Cl_2, the computed emission energy comes out $3814\,cm^{-1}$ too low as compared to experiment. Note that Su *et al.*[22] reported emission energies of $18\,509\,cm^{-1}$ and $18\,797\,cm^{-1}$ at the SO-CASPT2 and SO-CCSD(T) levels for UO_2Cl_2, respectively, also too low as compared to the experimental value of $20\,323\,cm^{-1}$. To check whether this discrepancy arises from the argon matrix, we have also performed TDDFT/CAM-B3LYP calculations on $UO_2Cl_2Ar_2$ used as a model for UO_2Cl_2 immersed in an Argon matrix and as evidenced by their SO-CCSD(T) calculations (Table 8 of Ref. 22) and our TDDFT/CAM-B3LYP ones (See Table S8) that both evidence that argon insignificantly modifies the transition energy. Therefore, we suspect that this inaccuracy for UO_2Cl_2 might be correlated with the underestimation observed for the bare uranyl molecule discussed earlier and requires a detailed investigation on its own.

For deep analysis, the vibronic progressions of the UO_2Cl_2 and $UO_2Cl_2(phen)_2$ complexes have been computed out of the first excited state to the ground state using their structures, as well as associated harmonic frequency spectra together with Hessian matrices. The main vibronic progression of uranium(VI) compounds is usually formed by the major contribution from the ground state symmetrical stretching mode coupling of the uranyl unit with minor contributions from other vibrational modes that depend on the complex structure and composition mainly. Here we are aiming at providing the assignment of visible spectral bands that were observed on emission spectra. On Figure 4 red curves correspond to experimental spectra of UO_2Cl_2 in Ar matrix at 4 K (top panel), $Cs_2UO_2Cl_4$ crystal at 80 K (middle panel) and $UO_2Cl_2(phen)_2$ at 80 K (bottom panel) while black vertical lines are corresponding theoretical vibronic progressions. For illustration purposes and clarity of comparison,

Table 6: SO-TDDFT emission energies (in cm^{-1}) and oscillator strengths of UO_2Cl_2 and $UO_2Cl_2(phen)_2$ computed at the PBE0-D3 geometries in the gas phase.

UO_2Cl_2		
Trans.	ΔE	f
$\sigma_u(37\%) + \mathrm{Cl}(45\%) \rightarrow \phi$	16 529	1.55×10^{-5}
$\sigma_u(37\%) + \mathrm{Cl}(45\%) \rightarrow \phi$	16 678	7.84×10^{-5}
$\sigma_u(37\%) + \mathrm{Cl}(45\%) \rightarrow \delta(50\%) + \phi(40\%)$	17 301	2.00×10^{-12}
$\sigma_u(37\%) + \mathrm{Cl}(45\%) \rightarrow \delta(56\%) + \phi(33\%)$	17 330	4.61×10^{-6}
$\sigma_u(37\%) + \mathrm{Cl}(45\%) \rightarrow \phi(49\%) + \delta(41\%)$	17 659	1.32×10^{-11}
$\sigma_u(37\%) + \mathrm{Cl}(45\%) \rightarrow \phi(54\%) + \delta(35\%)$	17 733	1.64×10^{-6}
$\sigma_u(37\%) + \mathrm{Cl}(45\%) \rightarrow \delta(82\%) + \phi(6\%)$	19 147	9.29×10^{-4}
$\sigma_u(37\%) + \mathrm{Cl}(45\%) \rightarrow \delta$	19 529	3.79×10^{-6}
$UO_2Cl_2(phen)_2$		
Trans.	ΔE	f
$\sigma_u + \mathrm{Cl} \rightarrow \phi(57\%) + \delta/\pi^*_{(phen)_{ax}}(14\%)$	18 464	1.23×10^{-4}
$\sigma_u + \mathrm{Cl} \rightarrow \phi(62\%) + \delta/\pi^*_{(phen)_{eq}}(20\%)$	18 629	3.33×10^{-5}
$\sigma_u + \mathrm{Cl} \rightarrow \delta/\pi^*_{(phen)_{ax}}(58\%) + \phi(3\%)$	18 919	7.71×10^{-9}
$\sigma_u + \mathrm{Cl} \rightarrow \delta/\pi^*_{(phen)_{ax}}(58\%)$	18 982	8.00×10^{-7}
$\sigma_u + \mathrm{Cl} \rightarrow \phi(79\%) + \delta/\pi^*_{(phen)_{eq}}(27\%)$	19 676	1.07×10^{-9}
$\sigma_u + \mathrm{Cl} \rightarrow \phi(62\%) + \delta/\pi^*_{(phen)_{eq}}(15\%)$	19 766	3.94×10^{-5}
$\sigma_u + \mathrm{Cl} \rightarrow \delta/\pi^*_{(phen)_{eq}}(30\%) + \delta/\pi^*_{(phen)_{eq}}(16\%)$	20 738	8.62×10^{-4}
$\sigma_u + \mathrm{Cl} \rightarrow \delta/\pi^*_{(phen)_{ax}}$	21 434	1.63×10^{-4}

both types of spectra were normalized by the maximum intensity value and theoretical ones were shifted to match the experimental luminescence origin. Figure 4 highlights the good agreement between the experimental and theoretical spectra since the band spacings of the computed vertical lines match nicely the experimental envelope.

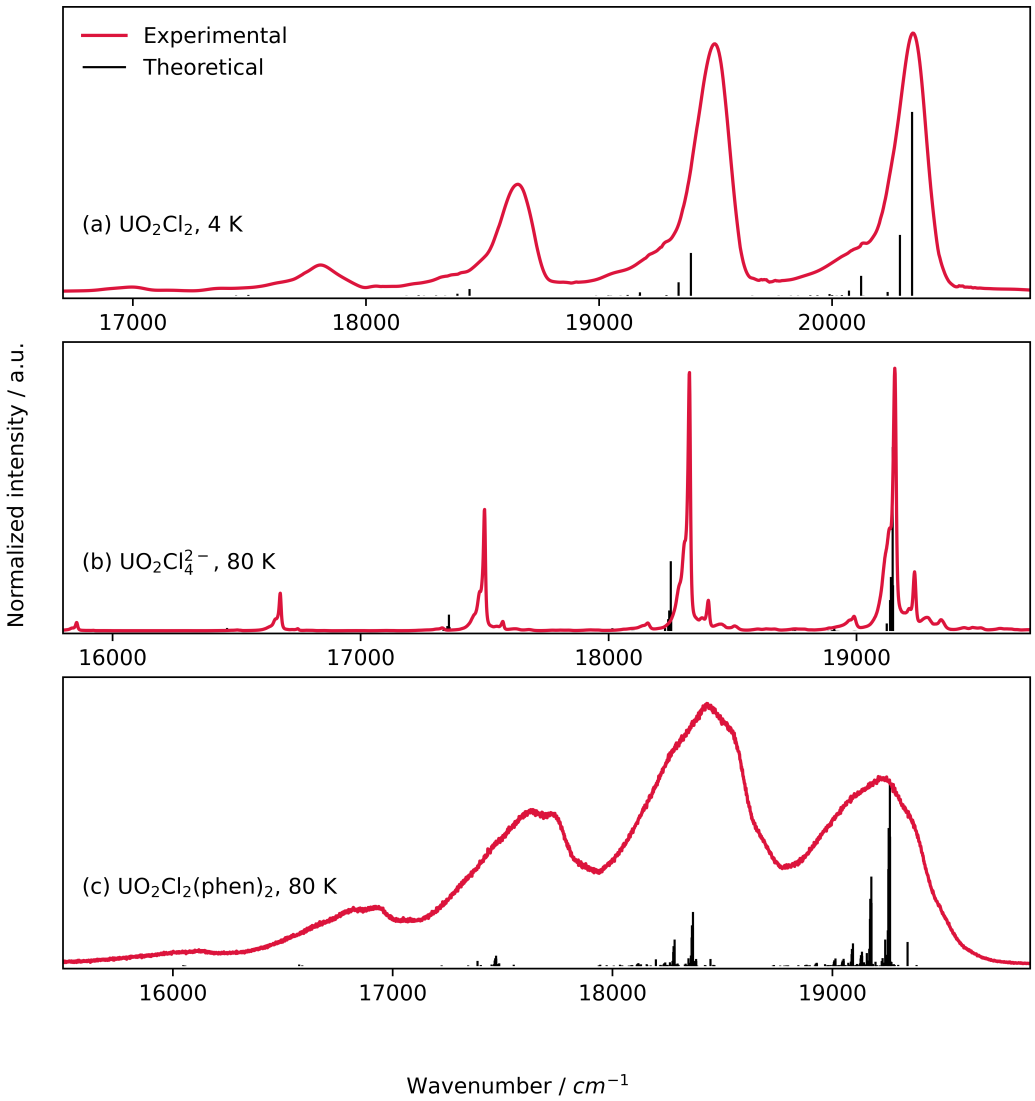

Figure 4: Comparison of theoretical and experimental luminescence spectra of (a) UO_2Cl_2,[64] reconstructed with permission from Jin *et al.*[64] – Copyright 2009 American Chemical Society; (b) $Cs_2UO_2Cl_4$ and (c) $UO_2Cl_2(phen)_2$ complexes. The origin of the theoretical spectrum is adjusted to match the experimental value.

The complete assignment of all obtained bands is provided in Supporting Information (Table S10 and Table S11). Here we discuss only significant differences between UO_2Cl_2, $UO_2Cl_4^{2-}$ and $UO_2Cl_2(phen)_2$ vibronic contributions. The first observed transition for all three compounds is computed to be 0'(0)→1(0) and corresponds to a 0 vibrational transition from excited to the ground state. The structure and symmetry of ligands in UO_2Cl_2 and $UO_2Cl_2(phen)_2$ complexes enable the uranyl bending mode to become vibronically excited and appear on the spectrum in the range of 219 to 281 cm^{-1}. Note that it is not the case for $UO_2Cl_4^{2-}$ complex because, in this energy region, the Cl−U−Cl symmetrical stretching mode contribution is observed. The analysis of other computed bands showed no other significant contributions than uranyl symmetrical stretching mode, which means that the coupling scheme remains the same for all uranium(VI) complexes discussed in this study. Here the ground state symmetrical stretching mode is computed to be placed at 949 cm^{-1}, 894 cm^{-1} and 895 cm^{-1} after 0'(0)→1(0) transition for UO_2Cl_2, $UO_2Cl_4^{2-}$ and $UO_2Cl_2(phen)_2$ respectively that is slightly overestimated as compared to averaged experimental band spacing of 840 cm^{-1}, 817 cm^{-1} and 794 cm^{-1}. Since theoretical band spacing is somewhat red-shifted one should note that anharmonicity corrections are not accounted for causing even bigger band shifts.

It is worth mentioning the broadening of experimental spectra. Despite the fact that the spectra were obtained at different low temperatures (4 and 80 K), as mentioned earlier, thermally active transitions do occur, but have been reduced to a minimum as much as possible. Their extent cannot be predicted, thus we eliminate direct comparison of UO_2Cl_2 broadening with $UO_2Cl_4^{2-}$ and $UO_2Cl_2(phen)_2$ ones. Nevertheless, we observe that in the spectra obtained at a temperature of 80 K, the width of the bands is not consistent. From the point of view of radioactive processes, if we refer to Figure 4 as well as to the assignment provided in Table S10, it can be seen visually that the number of bands in the 50 to 400 cm^{-1} region after 0'(0)→1(0) transition is much larger in the case of $UO_2Cl_2(phen)_2$ than in $UO_2Cl_4^{2-}$. This phenomenon could be explained by the uranyl bending mode coupling with

the ligands motions that are induced by the uranyl bent structure.

Conclusions

We have synthesized the bent $UO_2Cl_2(phen)_2$, confirming the structure reported by Schöne *et al.*[10]. The QC calculations provide a rationale for the geometry $UO_2Cl_2(phen)_2$. They demonstrate that the axial phenanthroline group largely contributes to making the bent actinyl structure energetically stable. QTAIM and NBO analysis however indicate the the nature of the $U-O_{yl}$ does not change upon bending, a fact that could be further investigated via quantum entanglement methods, as done by Leszczyk *et al.*[76]. In this study, we investigated the influence of the bending of the uranyl moiety and of the coordinated chloride and phenanthroline ligands with the help of spin-orbit coupled TDDFT calculations to determine the nature of the low-lying excited states of bare uranyl complexes versus that of uranyl tetrachloride, uranyl dichloride and the $UO_2Cl_2(phen)$. While in uranyl tetrachloride, the lowest electronic state causing luminescent emission has a predominant $5f_\delta$ character, the emitting state of all three complexes uranyl, UO_2Cl_2 and $UO_2Cl_2(phen)_2$ has a $5f_\phi$ character. The two chloride and phenanthroline ligands cause a larger destabilization of the ϕ states than of the δ states but at the same time a smaller SO splitting of the former than the latter. As a result, the energy gap between the lowest ϕ and δ SO states is as small as about $300\,cm^{-1}$, as opposed to $3000\,cm^{-1}$ in bare uranyl complexes.

Using SO-TDDFT/CAM-B3LYP calculations coupled with vibronic coupling simulations allows to compute the vibrational progressions of the emission spectra, for a direct comparison with the experimental spectra available for UO_2Cl_2 (though in Argon matrix), $Cs_2UO_2Cl_4$, and to the luminescence spectrum of $UO_2Cl_2(phen)_2$ measured for the first time at 80 K. Despite the need of shifting the origin of the computed spectrum with respect to the experimental one, the spacing between the computed vibronic bands match the experimental spectra envelopes. The presence of a bent uranyl moiety in UO_2Cl_2 and $UO_2Cl_2(phen)_2$ com-

plexes triggers vibronic excitations of the uranyl bending motion predominantly in the range of 219 to 281 cm^{-1}, broadening significantly the spectrum around the dominant progression that corresponds to the uranyl symmetric stretching mode. This broadening is a signature of the bending of uranyl, but it might also arise from motions of equatorial ligands, such as bromide in $UO_2Br_4{}^{2-}$. In practice, QC simulations have reached a reliable level of accuracy making it a first-choice methodology to discuss and assign emission spectra of uranyl complexes.

Acknowledgements

ASPG and VV acknowledge support from PIA ANR project CaPPA (ANR-11-LABX-0005-01), the Franco-German project CompRIXS (Agence nationale de la recherche ANR-19-CE29-0019, Deutsche Forschungsgemeinschaft JA 2329/6-1), I-SITE ULNE projects OVER-SEE and MESONM International Associated Laboratory (LAI) (ANR-16-IDEX-0004), the French Ministry of Higher Education and Research, region Hauts de France council and European Regional Development Fund (ERDF) project CPER CLIMIBIO, WaveTech and the French national supercomputing facilities (grants DARI A0130801859, A0110801859). HO, ASPG and VV also acknowledge funding by the ANR project ANR-21-CE29-0027. Experimental work was conducted at ANL, operated by UChicago Argonne LLC for the United States Department of Energy (U.S. DOE), and supported by the U.S. DOE Office of Science, Office of Basic Energy Sciences, Chemical Sciences Geological and Biosciences Division, Heavy Element Chemistry program under Contract DE-AC02-06CH11357. The authors acknowledge Sergey Telnov for his artistic contribution to graphical art.

Associated content

The data (input/output) corresponding to the QC calculations of this paper are available at the Zenodo repository.[77] The Supporting Information is available free of charge on the

ACS Publications website at DOI: XXX. Justification for performing the calculations in the gas-phase. Table summarizing the QTAIM and NBO data (Table S4), scalar relativistic transition energies (Table S5, Table S6, Table S7), comparison of TDDFT and TDA transition energies for UO_2Cl_2 and TDDFT energies of $UO_2Cl_2Ar_2$ (Table S8), TDDFT transition energies of $UO_2Cl_2(phen)_2$ computed at with the SR-ZORA Hamiltonian in the gas phase and the COSMO water solvent (Table S9), UO_2Cl_2, $UO_2Cl_4{}^{2-}$ and $UO_2Cl_2(phen)_2$ luminescence spectra assignment computed in the gas-phase at 4K (Table S10, Table S11). The FT-IR and Raman spectra of $UO_2Cl_2(phen)_2$ under ^{18}O exchange (Figure S1, Figure S2).

References

(1) Grenthe, I.; Drożdżyński, J.; Fujino, T.; Buck, E. C.; Albrecht-Schmitt, T. E.; Wolf, S. F. In *The Chemistry of the Actinide and Transactinide Elements*, 3rd ed.; Morss, L. R., Edelstein, N. M., Fuger, J., Eds.; Springer: Dordrecht, The Netherlands, 2006; Chapter 5, pp 253–698, DOI: 10.1007/1-4020-3598-5_5.

(2) Hayton, T. W. Understanding the origins of $O_{yl}-U-O_{yl}$ bending in the uranyl (UO_2^{2+}) ion. *Dalton Trans.* **2018**, *47*, 1003–1009, DOI: 10.1039/c7dt04123c.

(3) Dyall, K. G. Bonding and bending in the actinyls. *Mol. Phys.* **1999**, *96*, 511, DOI: 10.1080/00268979909482988.

(4) Sunaga, A.; Tabata, C.; Yamamura, T. Linearity and Chemical Bond of UO_2^{2+} Revisited: A Comparison Study with UN_2 and UE_2^{2+} (E = S, Se, and Te) Based on Relativistic Calculations. *J. Phys. Chem. A* **2022**, *126*, 8606–8617, DOI: 10.1021/acs.jpca.2c05216.

(5) Hratchian, H. P.; Sonnenberg, J. L.; Hay, P. J.; Martin, R. L.; Bursten, B. E.; Schlegel, H. B. Theoretical investigation of uranyl dihydroxide: oxo ligand exchange, water catalysis, and vibrational spectra. *J. Phys. Chem. A* **2005**, *109*, 8579–8586, DOI: 10.1021/jp052616m.

(6) Schreckenbach, G.; Hay, P. J.; Martin, R. L. Theoretical study of stable trans and cis isomers in $[UO_2(OH)_4]^{2-}$ using relativistic density functional theory. *Inorg. Chem.* **1998**, *37*, 4442, DOI: 10.1021/ic980057a.

(7) Schreckenbach, G.; Hay, P. J.; Martin, R. L. Density functional calculations on actinide compounds: survey of recent progess and application to $[UO_2X_2]^{2-}$ (X=F, Cl, OH) and AnF_6 (An = U, Np, Pu). *J. Comp. Chem.* **1999**, *20*, 70–90, DOI: 10.1002/(SICI)1096-987X(19990115)20:1<70::AID-JCC9>3.0.CO;2-F.

(8) Vallet, V.; Wahlgren, U.; Grenthe, I. Probing the Nature of Chemical Bonding in Uranyl(VI) Complexes with Quantum Chemical Methods. *J. Phys. Chem. A* **2012**, *116*, 12373–12380, DOI: 10.1021/jp3091123.

(9) Pietro, P. D.; Kerridge, A. $U-O_{yl}$ Stretching Vibrations as a Quantitative Measure of the Equatorial Bond Covalency in Uranyl Complexes: A Quantum-Chemical Investigation. *Inorg. Chem.* **2016**, *55*, 573–583, DOI: 10.1021/acs.inorgchem.5b01219.

(10) Schöne, S.; Radoske, T.; März, J.; Stumpf, T.; Patzschke, M.; Ikeda-Ohno, A. $[UO_2Cl_2(phen)_2]$, a Simple Uranium(VI) Compound with a Significantly Bent Uranyl Unit (phen = 1,10-phenanthroline). *Chem. Eur. J.* **2017**, *23*, 13574–13578, DOI: 10.1002/chem.201703009.

(11) Langer, E. M.; Kegler, P.; Kowalski, P. M.; Wang, S.; Alekseev, E. V. Achieving and Stabilizing Uranyl Bending via Physical Pressure. *Inorg. Chem.* **2021**, *60*, 8419–8422, DOI: 10.1021/acs.inorgchem.1c00644.

(12) Probing the Influence of N-Donor Capping Ligands on Supramolecular Assembly in Molecular Uranyl Materials. *Eur. J. Inorg. Chem.* **2016**, *2016*, 126–137, DOI: 10.1002/ejic.201501118.

(13) Carter, K. P.; Kalaj, M.; Kerridge, A.; Ridenour, J. A.; Cahill, C. L. How to Bend the Uranyl Cation via Crystal Engineering. *Inorg. Chem.* **2018**, *57*, 2714–2723, DOI: 10.1021/acs.inorgchem.7b03080, PMID: 29436823.

(14) Zhang, Z.; Pitzer, R. M. Application of relativistic quantum chemistry to the electronic energy levels of the uranyl ion. *J. Phys. Chem. A* **1999**, *103*, 6880–6886, DOI: 10.1021/jp991867q.

(15) Denning, R. G. *Complexes, Clusters and Crystal Chemistry*; Sringer, 1992; Vol. 79; pp 215–276, DOI: 10.1007/BFb0036502.

(16) Denning, R. G. Electronic structure and bonding in actinyl ions and their analogs. *J. Phys. Chem. A* **2007**, *111*, 4125–4143, DOI: 10.1021/jp071061n.

(17) Matsika, S.; Pitzer, R. M. Actinyl ions in $Cs_2UO_2Cl_4$. *J. Phys. Chem. A* **2001**, *105*, 637–645, DOI: 10.1021/jp003032h.

(18) Réal, F.; Gomes, A. S. P.; Visscher, L.; Vallet, V.; Eliav, E. Benchmarking Electronic Structure Calculations on the Bare $UO_2{}^{2+}$ ion: How Different are Single and Multireference Electron Correlation Methods? *J. Phys. Chem. A* **2009**, *113*, 12504–12511, DOI: 10.1021/jp903758c.

(19) Pierloot, K.; van Besien, E. Electronic structure and spectrum of UO_2^{2+} and $UO_2Cl_4^{2-}$. *J. Chem. Phys.* **2005**, *123*, 204309, DOI: 10.1063/1.2121608.

(20) Réal, F.; Vallet, V.; Marian, C.; Wahlgren, U. Theoretical investigation of the energies and geometries of photo-excited uranyl(VI) ion: a comparison between wavefunction theory and density functional theory. *J. Chem. Phys.* **2007**, *127*, 214302, DOI: 10.1063/1.2814157.

(21) Tecmer, P.; Gomes, A. S. P.; Ekström, U.; Visscher, L. Electronic Spectroscopy of $UO_2{}^{2+}$, NUN and NUO^+. *Phys. Chem. Chem. Phys.* **2011**, *13*, 6249–6259, DOI: 10.1039/c0cp02534h.

(22) Su, J.; Wang, Y.-L.; Wei, F.; Schwarz, W. H. E.; Li, J. Theoretical Study of the Luminescent States and Electronic Spectra of UO_2Cl_2 in an Argon Matrix. *J. Chem. Theory Comput.* **2011**, *7*, 3293–3303, DOI: 10.1021/ct200419x.

(23) Shen, G.; Guo, M.; Wang, Z.; Wang, F. Effects of ligands on excitation energies of $[UO_2X_4]^{2-}$ and UO_2X_2(X = F, Cl) with the equation-of-motion coupled-cluster theory. *Int. J. Quantum Chem.* **2022**, *122*, e26981, DOI: 10.1002/qua.26981.

(24) Kaltsoyannis, N.; Hay, P. J.; Li, J.; Blaudeau, J.-P.; Bursten, B. E. In *The Chemistry of the Actinide and Transactinide Elements*, 4th ed.; Morss, L. R., Edelstein, N. M., Fuger, J., Eds.; Springer: Dordrecht, The Netherlands, 2010; Vol. 3; Chapter 17, pp 1893–2012, DOI: 10.1007/978-94-007-0211-0_17.

(25) Gomes, A. S. P.; Réal, F.; Schimmelpfennig, B.; Wahlgren, U.; Vallet, V. In *Computational Methods in Lanthanide and Actinide Chemistry*; Dolg, M., Ed.; John Wiley & Sons Ltd, 2015; Chapter 11, pp 269–298, DOI: 10.1002/9781118688304.ch11.

(26) Leszczyk, A.; Tecmer, P.; Boguslawski, K. In *Transition Metals in Coordination Environments. Challenges and Advances in Computational Chemistry and Physics*; Broclawik E., R. M., Borowski T., Ed.; Springer, 2019; Vol. 29; pp 121–160, DOI: 10.1007/978-3-030-11714-6_5.

(27) Réal, F.; Vallet, V.; Wahlgren, U.; Grenthe, I. *Ab initio* study of the mechanism for photoinduced yl-oxygen exchange in uranyl(VI) in acidic aqueous solution. *J. Am. Chem. Soc.* **2008**, *130*, 11742–11751, DOI: 10.1021/ja8026407.

(28) Su, J.; Wang, Z.; Pan, D.; Li, J. Excited States and Luminescent Properties of UO_2F_2 and Its Solvated Complexes in Aqueous Solution. *Inorg. Chem.* **2014**, *53*, 7340–7350, DOI: 10.1021/ic5006852.

(29) van Besien, E.; Pierloot, K.; Görller-Walrand Electronic spectra of uranyl chloride complexes in acetone: a CASSCF/CASPT2 investigation. *Phys. Chem. Chem. Phys.* **2006**, *8*, 4311–4319, DOI: 10.1039/b607026d.

(30) Pierloot, K.; van Besien, E.; van Lenthe, E.; Baerends, E. J. Electronic structure and spectrum of UO_2^{2+} and $UO_2Cl_4^{2-}$ calculated with time-dependent density functional theory. *J. Chem. Phys.* **2007**, *126*, 194311, DOI: 10.1063/1.2735297.

(31) Gomes, A. S. P.; Jacob, C. R.; Réal, F.; Visscher, L.; Vallet, V. Towards systematically improvable models for actinides in condensed phase: the electronic spectrum of uranyl

in $Cs_2UO_2Cl_4$ as a test case. *Phys. Chem. Chem. Phys.* **2013**, *15*, 15153–15162, DOI: 10.1039/C3CP52090K.

(32) Frisch, M. J.; Trucks, G. W.; Schlegel, H. B.; Scuseria, G. E.; Robb, M. A.; Cheeseman, J. R.; Scalmani, G.; Barone, V.; Petersson, G. A.; Nakatsuji, H.; Li, X.; Caricato, M.; Marenich, A. V.; Bloino, J.; Janesko, B. G.; Gomperts, R.; Mennucci, B.; Hratchian, H. P.; Ortiz, J. V.; Izmaylov, A. F.; Sonnenberg, J. L.; Williams-Young, D.; Ding, F.; Lipparini, F.; Egidi, F.; Goings, J.; Peng, B.; Petrone, A.; Henderson, T.; Ranasinghe, D.; Zakrzewski, V. G.; Gao, J.; Rega, N.; Zheng, G.; Liang, W.; Hada, M.; Ehara, M.; Toyota, K.; Fukuda, R.; Hasegawa, J.; Ishida, M.; Nakajima, T.; Honda, Y.; Kitao, O.; Nakai, H.; Vreven, T.; Throssell, K.; Montgomery, J. A., Jr.; Peralta, J. E.; Ogliaro, F.; Bearpark, M. J.; Heyd, J. J.; Brothers, E. N.; Kudin, K. N.; Staroverov, V. N.; Keith, T. A.; Kobayashi, R.; Normand, J.; Raghavachari, K.; Rendell, A. P.; Burant, J. C.; Iyengar, S. S.; Tomasi, J.; Cossi, M.; Millam, J. M.; Klene, M.; Adamo, C.; Cammi, R.; Ochterski, J. W.; Martin, R. L.; Morokuma, K.; Farkas, O.; Foresman, J. B.; Fox, D. J. Gaussian~16 Revision C.01. 2016; Gaussian Inc. Wallingford CT.

(33) Perdew, J. P.; Burke, K.; Ernzerhof, M. Generalized gradient approximation made simple. *Phys. Rev. Lett.* **1996**, *77*, 3865–3868, DOI: 10.1103/PhysRevLett.77.3865.

(34) Adamo, C.; Barone, V. Toward reliable density functional methods without adjustable parameters: The PBE0 model. *J. Chem. Phys.* **1999**, *110*, 6158–6170, DOI: 10.1063/1.478522.

(35) Grimme, S.; Antony, J.; Ehrlich, S.; Krieg, H. A consistent and accurate ab initio parametrization of density functional dispersion correction (DFT-D) for the 94 elements H-Pu. *J. Chem. Phys.* **2010**, *132*, 154104, DOI: 10.1063/1.3382344.

(36) Grimme, S.; Ehrlich, S.; Goerigk, L. Effect of the damping function in dispersion

corrected density functional theory. *J. Comput. Chem.* **2011**, *32*, 1456–1465, DOI: 10.1002/jcc.21759.

(37) Küchle, W.; Dolg, M.; Stoll, H.; Preuss, H. Energy-adjusted pseudopotentials for the actinides. Parameter sets and test calculations for thorium and thorium monoxide. *J. Chem. Phys.* **1994**, *100*, 7535, DOI: 10.1063/1.466847.

(38) Cao, X.; Dolg, M.; Stoll, H. Valence basis sets for relativistic energy-consistent small-core actinide pseudopotentials. *J. Chem. Phys.* **2003**, *118*, 487, DOI: 10.1063/1.1521431.

(39) Cao, X.; Dolg, M. Segmented contraction scheme for small-core actinide pseudopotential basis sets. *J. Mol. Struct. (Theochem)* **2004**, *673*, 203–209, DOI: 10.1016/j.theochem.2003.12.015.

(40) Weigend, F.; Ahlrichs, R. Balanced basis sets of split valence, triple zeta valence and quadruple zeta valence quality for H to Rn: Design and assessment of accuracy. *Phys. Chem. Chem. Phys.* **2005**, *7*, 3297–3305, DOI: 10.1039/B508541A.

(41) Gutowski, K. E.; Dixon, D. A. Predicting the Energy of the Water Exchange Reaction and Free Energy of Solvation for the Uranyl Ion in Aqueous Solution. *J. Phys. Chem. A* **2006**, *110*, 8840–8856, DOI: 10.1021/jp061851h.

(42) Wåhlin, P.; Danilo, C.; Vallet, V.; Réal, F.; Flament, J.-P.; Wahlgren, U. An investigation of the accuracy of different DFT functionals on the water exchange reaction in hydrated uranyl(VI) in the ground state and the first excited state. *J. Chem. Theory Comput.* **2008**, *4*, 569–577, DOI: 10.1021/ct700062x.

(43) Austin, J. P.; Burton, N. A.; Hillier, I. H.; Sundararajan, M.; Vincent, M. A. Which density functional should be used to study actinyl complexes? *Phys. Chem. Chem. Phys.* **2009**, *11*, 1143–1145, DOI: 10.1039/b821577d.

(44) Bader, R. F. W. A Quantum Theory of Molecular Structure and Its Application. *Chem. Rev.* **1991**, *91*, 893–928, DOI: 10.1021/cr00005a013.

(45) Bader, R. F. W. *Atoms in Molecules - A Quantum Theory*; Oxford University Press, 1994.

(46) Keith, T. A. AIMAll (version 19.10.12), Todd A. Keith, TK Gristmill Software: Overland Park KS, 2019. http://aim.tkgristmill.com.

(47) Glendening, E. D.; Badenhoop, J. K.; Reed, A. E.; Carpenter, J. E.; Bohmann, J. A.; Morales, C. M.; Karafiloglou, P.; Landis, C. R.; Weinhold, F. NBO 7.0. 2018.

(48) Yanai, T.; Tew, D. P.; Handy, N. C. A new hybrid exchange-correlation functional using the Coulomb-attenuating method (CAM-B3LYP). *Chem. Phys. Lett.* **2004**, *393*, 51–57, DOI: 10.1016/j.cplett.2004.06.011.

(49) Tecmer, P.; Bast, R.; Ruud, K.; Visscher, L. Charge-Transfer Excitations in Uranyl Tetrachloride ($[UO_2Cl_4]^{2-}$): How Reliable are Electronic Spectra from Relativistic Time-Dependent Density Functional Theory? *J. Phys. Chem. A* **2012**, *116*, 7397–7404, DOI: 10.1021/jp3011266.

(50) Tecmer, P.; Govind, N.; Kowalski, K.; de Jong, W. A.; Visscher, L. Reliable modeling of the electronic spectra of realistic uranium complexes. *J. Chem. Phys.* **2013**, *139*, 034301, DOI: 10.1063/1.4812360.

(51) Oher, H.; Réal, F.; Vercouter, T.; Vallet, V. Investigation of the Luminescence of $[UO_2X_4]^{2-}$ (X = Cl, Br) Complexes in the Organic Phase Using Time-Resolved Laser-Induced Fluorescence Spectroscopy and Quantum Chemical Simulations. *Inorg. Chem.* **2020**, *59*, 5896–5906, DOI: 10.1021/acs.inorgchem.9b03614.

(52) Oher, H.; Vercouter, T.; Réal, F.; Shang, C.; Reiller, P. E.; Vallet, V. Influence of alkaline earth metal ions on structures and luminescent properties of

$Na_mMe_nUO_2(CO_3)_3^{(4-m-2n)-}$ (Me = Mg, Ca; m, n = 0-2): time-resolved fluorescence spectroscopy and ab initio studies. *Inorg. Chem.* **2020**, *59*, 15036–15049, DOI: 10.1021/acs.inorgchem.0c01986.

(53) Oher, H.; Ferru, G.; Couston, L.; Berthon, L.; Guillaumont, D.; Réal, F.; Vercouter, T.; Vallet, V. Influence of the first coordination of uranyl on its luminescence properties: study of uranyl binitrate with N,N-dialkyl amide DEHiBA and water. *Inorg. Chem.* **2022**, *61*, 890–901, DOI: 10.1021/acs.inorgchem.1c02618.

(54) Yang, J.-J.; Zhao, Z.; Su, J. Theoretical Study of the Excited States and Luminescent Properties of $(H_2O)nUO_2Cl_2$ (n = 1–3). *Inorg. Chem.* **2023**, *62*, 1978–1987, DOI: 10.1021/acs.inorgchem.2c03249.

(55) Misael, W. A.; Gomes, A. S. P. 2023, DOI: 10.48550/ARXIV.2302.07223.

(56) Fonseca Guerra, C.; Snijders, J. G.; te Velde, G.; Baerends, E. J. *Theor. Chem. Acc.* **1998**, *99*, 391–403, DOI: 10.1007/s002149800m26.

(57) te Velde, G.; Bickelhaupt, F. M.; Baerends, E. J.; Fonseca Guerra, C.; van Gisbergen, S. J. A.; Snijders, J. G.; Ziegler, T. Chemistry with ADF. *J. Comput. Chem.* **2001**, *22*, 931–967, DOI: 10.1002/jcc.1056.

(58) ADF2021.106. http://www.scm.com.

(59) van Lenthe, E.; Baerends, E. J.; Snidjers, J. G. Relativistic regular two-component Hamiltonians. *J. Chem. Phys.* **1993**, *99*, 4597–4610, DOI: 10.1063/1.466059.

(60) van Lenthe, E.; Baerends, E. J.; Snidjers, J. G. Relativistic total energy using regular approximations. *J. Chem. Phys.* **1994**, *101*, 9783–9792, DOI: 10.1063/1.467943.

(61) van Lenthe, E.; Ehlers, A.; Baerends, E. J. Geometry optimizations in the zero order regular approximation for relativistic effects. *J. Chem. Phys.* **1999**, *110*, 8943–8953, DOI: 10.1063/1.478813.

(62) Van Lenthe, E.; Baerends, E. J. Optimized Slater-type basis sets for the elements 1–118. *J. Comput. Chem.* **2003**, *24*, 1142–1156, DOI: 10.1002/jcc.10255.

(63) Mozhayskiy, V.; Krylov, A. ezSpectrum, http://iopenshell.usc.edu/downloads. http://iopenshell.usc.edu/downloads.

(64) Jin, J.; Gondalia, R.; Heaven, M. C. Electronic Spectroscopy of UO_2Cl_2 Isolated in Solid Ar. *J. Phys. Chem. A* **2009**, *113*, 12724–12728, DOI: 10.1021/jp9052133.

(65) Schnaars, D. D.; Wilson, R. E. Lattice Solvent and Crystal Phase Effects on the Vibrational Spectra of $UO_2Cl_4^{2-}$. *Inorg. Chem.* **2014**, *53*, 11036–11045, DOI: 10.1021/ic501553m.

(66) Schnaars, D. D.; Wilson, R. E. Structural and vibrational properties of $U(VI)O_2Cl_4^{2-}$ and $Pu(VI)O_2Cl_4^{2-}$ Complexes. *Inorg. Chem.* **2013**, *52*, 14138–14147, DOI: 10.1021/ic401991n.

(67) Sheldrick, G. M. SADABS, Program for Empirical Absorption Correction of Area Detector Data. 1996.

(68) Sheldrick, G. M. A Short History of SHELX. *Acta Crystallogr. A* **2008**, *64*, 112–122, DOI: 10.1107/S0108767307043930.

(69) Wadt, W. R. Why UO_2^{2+} is linear and isoelectronic ThO_2 is bent? *J. Am. Chem. Soc.* **1981**, *103*, 6053, DOI: 10.1021/ja00410a011.

(70) Tatsumi, K.; Hoffmann, R. Bent cis d^0 MoO_2^{2+} vs linear trans d^0f^0 UO_2^{2+}: A significant role for nonvalence 6p orbitals in uranyl. *Inorg. Chem.* **1980**, *20*, 1950, DOI: 10.1021/ic50211a035.

(71) Su, J.; Dau, P. D.; Qiu, Y.-H.; Liu, H.-T.; Xu, C.-F.; Huang, D.-L.; Wang, L.-S.; Li, J. Probing the Electronic Structure and Chemical Bonding in Tricoordinated Uranyl

Complexes $UO_2X_3^-$ (X=F, Cl, Br, I): Competition between Coulomb Repulsion and U-X Bonding. *Inorg. Chem.* **2013**, *52*, 6617–6626, DOI: 10.1021/ic4006482.

(72) Ruipérez, F.; Wahlgren, U. Charge transfer in uranyl(VI) halides $[UO_2X_4]^{2-}$ (X = F, Cl, Br and I). A quantum chemical study of the absorption spectra. *J. Phys. Chem. A* **2010**, *114*, 3615–3621, DOI: 10.1021/jp911271q.

(73) (a) Dreuw, A.; Head-Gordon, M. Failure of Time-Dependent Density Functional Theory for Long-Range Charge-Transfer Excited States: The Zincbacteriochlorin-Bacteriochlorin and Bacteriochlorophyll-Spheroidene Complexes. *J. Am. Chem. Soc.* **2004**, *126*, 4007–4016, DOI: 10.1021/ja039556n; (b) Eriksen, J. J.; Sauer, S. P.; Mikkelsen, K. V.; Christiansen, O.; Jensen, H. J. A.; Kongsted, J. Failures of TDDFT in describing the lowest intramolecular charge-transfer excitation in para-nitroaniline. *Mol. Phys.* **2013**, *111*, 1235–1248, DOI: 10.1080/00268976.2013.793841.

(74) Wang, Z.; M. Zachara, J.; Liu, C.; Gassman, P.; R. Felmy, A.; B. Clark, S. A cryogenic fluorescence spectroscopic study of uranyl carbonate, phosphate and oxyhydroxide minerals. *Radiochim. Acta* **2008**, *96*, 591–598, DOI: 10.1021/es048448d.

(75) Denning, R. G.; Snellgrove, T. R.; Woodwark, D. R. The electronic structure of the uranyl ion: Part I. The electronic spectrum of $Cs_2UO_2Cl_4$. *Mol. Phys.* **1976**, *32*, 419–442, DOI: 10.1080/00268977600103211.

(76) Leszczyk, A.; Dome, T.; Tecmer, P.; Kedziera, D.; Boguslawski, K. Resolving the π-assisted U–N σ_f-bond formation using quantum information theory. *Phys. Chem. Chem. Phys.* **2022**, *24*, 21296–21307, DOI: 10.1039/D2CP03377A.

(77) Oher, H.; Gomes, A. S. P.; Wilson, R. E.; Schnaars, D.; Vallet, V. Dataset: Does the bending of uranyl influence its spectroscopy and luminescence. 2023; https://doi.org/10.5281/zenodo.7702591.

TOC Graphic

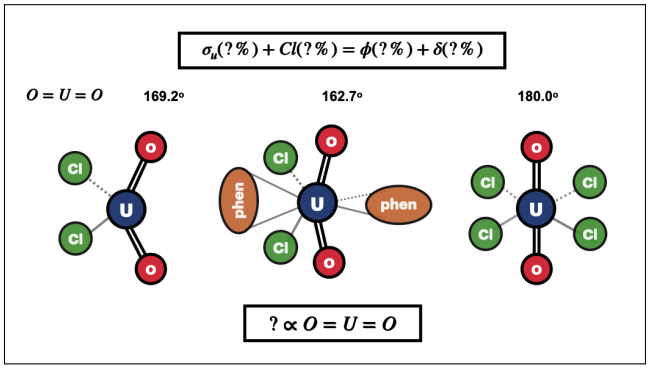

The luminescence spectrum of a bent uranyl complex with chloride ligands and 1,10-phenanthroline ligands has been experimentally recorded for the first time, and also successfully computed by vibrationally resolved ab initio calculations. Notably, we demonstrate that the bending of uranyl in $UO_2Cl_2(phen)_2$ and in the UO_2Cl_2 complex triggers vibronically induced excitations of the uranyl bending mode, yielding denser luminescence spectra than in linear uranyl complexes.